Electronic Supplementary Material (ESI) for Physical Chemistry Chemical Physics.
This journal is © the Owner Societies 2015

Supplementary Information:

Pore Collapse and Regrowth in Silicon Electrodes for Rechargeable Batteries

Steven C. DeCaluwe[2,3,4], Bal Mukund Dhar*[1,5], Liwei Huang[1], Yuping He[1,6], Kaikun Yang[1], Jon P. Owejan[7], Yiping Zhao[6], A. Alec Talin[8,9], Joseph A. Dura†[3], Howard Wang†[1,4,5]*

1. Institute for Materials Research and Dept. of Mechanical Engineering, State University of New York, Binghamton, NY, United States
2. Department of Mechanical Engineering, Colorado School of Mines, Golden, CO, United States.
3. Center for Neutron Research, National Institute of Standards and Technology, Gaithersburg, MD, United States.
4. Department of Materials Science and Engineering, University of Maryland, College Park, MD, United States.
5. Material Measurement Laboratory, National Institute of Standards and Technology, Gaithersburg, MD, United States.
6. Department of Physics and Astronomy, University of Georgia, Athens, GA, United States
7. Department of Mechanical and Electrical Engineering Technology, State University of New York, Alfred, NY, United States.
8. Center for Nanoscale Science and Technology, National Institute of Standards and Technology, Gaithersburg, MD, United States.
9. Sandia National Laboratories, Livermore, CA, United States.

* These authors contributed equally to this work.

† Corresponding author

Supplementary Information

EIS Fitting Details

Table S1 provides the full set of fitting parameters for equivalent circuit fits to EIS data at each test point. Throughout the supplement, numbers in brackets, ± values, and figure error bars represent 68% confidence intervals. Parameters are given for fits to EIS taken in the "initial" state, immediately after the galvanostatic charge/discharge and for fits to EIS taken in the "relaxed" state, up to several hours after charge/discharge. In the delithiated state, there was significant frequency overlap between the a-Si and double layer elements for the initial EIS data, and this data was best fit by a circuit that omitted the double layer element. As mentioned in the manuscript, due to beamtime restrictions the last EIS data set for test point C6 was taken only 21

Table S1: Analysis of EIS for varying state-of-charge.

	OC initial	OC relaxed	D1 initial	D1 relaxed	C1 initial	C1 relaxed	D6 initial	D6 relaxed	C6 initial	C6 partially relaxed
Electrolyte: R_{Elec} (Ω)	29.4 ±0.8	28.0 ±0.9	12.9 ±10.0	15.8 ±10.5	28.0 ±0.8	27.0 ±12.3	28.5 ±14.7	42.1 ±9.9	27.2 ±1.2	27.0 ±1.0
Interfacial layers: R_{Int} (Ω)	211.8 ±2.4	126.1 ±1.3	129.3 ±9.9	131.4 ±1.5	139.7 ±1.5	177.6 ±15.5	179.4 ±27.4	186.1 ±34.1	224.9 ±2.5	210.7 ±3.0
Q_{Int} (μS-s^n)	3.10 ±0.62	0.72 ±0.03	0.26 ±0.05	0.50 ±0.10	2.46 ±0.56	5.50 ±2.30	3.75 ±2.86	3.74 ±2.70	1.75 ±0.39	1.69 ±0.39
n_{Int}	0.56 ±0.02	0.64 ±0.01	0.69 ±0.00	0.66 ±0.02	0.57 ±0.02	0.52 ±0.04	0.55 ±0.07	0.58 ±0.07	0.58 ±0.02	0.58 ±0.02
$\omega_{\mathrm{max,Int}}$ (rad/s)	0.50e6	1.99e6	3.15e6	1.99e6	1.25e6	0.63e6	0.63e6	0.25e6	0.79e6	0.79e6
C_{Int} (nF)	10.1 ±2.9	4.1 ±0.7	2.7 ±0.5	3.4 ±1.3	5.5 ±1.8	9.2 ±6.5	9.2 ±11.1	20.4 ±22.4	5.8 ±1.8	5.8 ±1.9
a-Si: R_{Si} (Ω)	3992.0 ±73.8	1145.0 ±20.2	49.2 ±2.5	60.1 ±5.3	7783.0 ±142.2	1153.0 ±36.0	57.4 ±17.3	62.3 ±20.6	3633.0 ±144.0	4944.0 ±137.8
Q_{Si} (μS-s^n)	96.3 ±1.0	126.0 ±5.2	468.0 ±185.0	657.0 ±249.0	82.2 ±0.7	94.1 ±0.5	535.0 ±294.0	465.0 ±269.0	238.0 ±12.7	263.0 ±3.0
n_{Si}	0.78 ±0.01	0.74 ±0.01	0.56 ±0.05	0.54 ±0.07	0.79 ±0.01	0.76 ±0.01	0.57 ±0.14	0.51 ±0.21	0.62 ±0.01	0.57 ±0.00
$\omega_{\mathrm{max,Si}}$ (rad/s)	3.15	12.5	791.0	395.5	1.58	19.8	499.1	993.5	1.3	0.63
C_{Si} (μF)	74.8 ±1.5	66.0 ±3.2	24.7 ±12.8	42.2 ±23.7	74.7 ±0.8	45.5 ±1.8	35.9 ±37.5	15.8 ±25.0	218.7 ±11.7	321.0 ±3.7
Double layer*: Q_{dl} (S-s^n)	--	3.76 e-3 ±6.4e-7	7.22e-3 ±2.12e-4	6.83e-3 ±2.02e-4	--	2.84e-3 ±1.72e-4	4.28e-3 ±2.68e-4	4.67e-3 ±3.21e-4	--	--
n_{dl}	--	0.96 ±0.01	0.64 ±0.02	0.72 ±0.02	--	0.84 ±0.07	0.72 ±0.02	0.73 ±0.05	--	--

*At low frequencies and high impedance the double layer feature is obscured by the higher impedance of the a-Si. Therefore for certain cases the double layer (CPE in series) was eliminated from the equivalent circuit model.

minutes after charge, and this state is specified as "partialy relaxed." As with the initial data, the a-Si and double layer circuit elements could not be resolved as separate entities for this data set, due to frequency overlap. The a-Si circuit elements parameters for "C6 partially relaxed" therefore compensate for some portion of the missing double layer circuit element in the fit, and consequently these results are not incorporated in the subsequent analysis. The pseudo-capacitance values C_{Int} and C_{Si} in Table S1 were calculated according to:

$$C = Q^{\text{o}}(\omega_{\text{max}})^{n-1} \tag{S1}$$

where Q^{o} is equal to the admittance (1/|Z|) at ω = 1 rad/s, ω_{max} is the peak frequency where the imaginary impedance is minimized, and n is the ideality factor of the CPE.

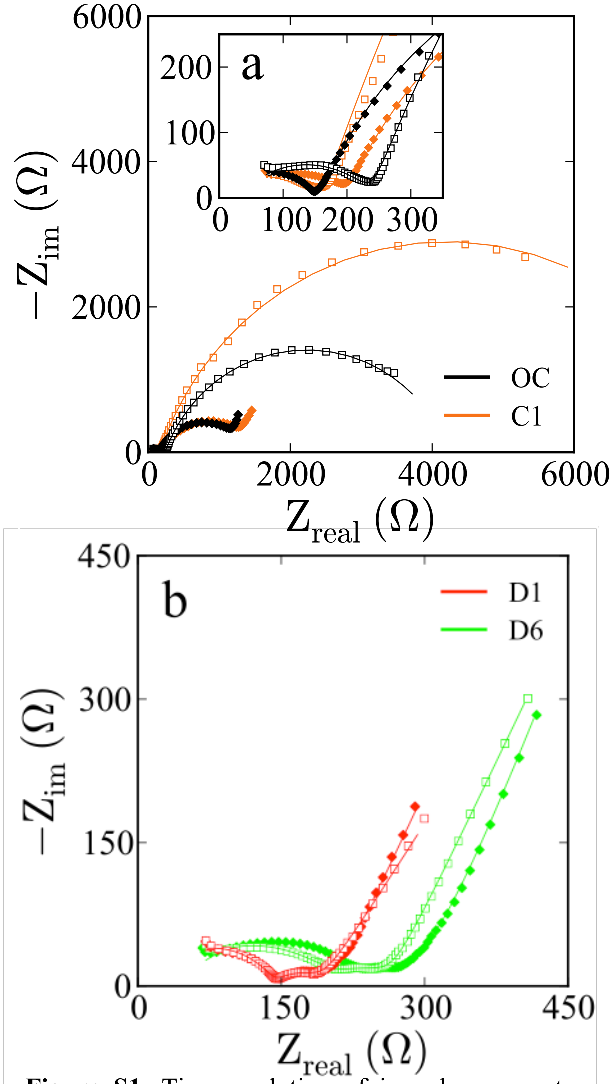

Figure S1. Time evolution of impedance spectra. Open symbols represent the initial state, just after the galvanostatic charge/discharge step, and filled symbols represent the relaxed state. (a) Delithiated states OC, C1, and C6. The 'C6 relaxed' state is only partially relaxed. Results show significant "relaxation" of the EIS with time; (b) Lithiated states D1 and D6. No significant relaxation of the EIS is observed.

EIS "Relaxation" in the Delithiated State

As discussed in the main body of the manuscript and demonstrated in Table S1, significant transient phenomena were observed in the EIS data. Figure S1 shows the time evolution of impedance spectra of the cell at different states of charge (SOC), comparing the initial state (open symbols) and relaxed state (filled symbols), along with the fits to each (solid lines). Because the relaxed EIS data for C6 was not available, this test point is omitted from this analysis. Figure S1(a) shows spectra for the delithiated states (OC and C1), with the inset focusing on the high frequency data, and Figure S1(b) shows spectra for the lithiated states (D1 and D6). Results in Figure S1(a) demonstrate significant relaxation in the delithiated states, with a notable reduction in impedance values after several hours at open circuit. As seen in Figure S1(b), no significant relaxation is observed in the lithiated state.

Figure S2 shows the time evolution of the a-Si layer resistance R_{Si} in Figure S2(a) and the pseudo-capacitance C_{Si} in Figure S2(b). While there were differences in the initial and relaxed values for other fitting parameters, the differences were small and did not show any consistent trend with test point or SOC. Results show that the Si resistance increases to values ≥ 4000 Ω immediately after delithiation, and relaxes consistently to a value between 1117 and 1189 Ω, roughly 20 times greater than for the lithiated states. The fitted capacitance values also decrease with time after delithiation, though not to the same degree as for the resistance values. While the capacitance is generally higher in the delithiated states than in the lithiated states, the capacitance differences are much smaller than the corresponding resistance differences. The larger error bars on the lithiated capacitance values (because of significant frequency overlap between adjacent equivalent circuit elements in these states) prevent any meaningful conclusions

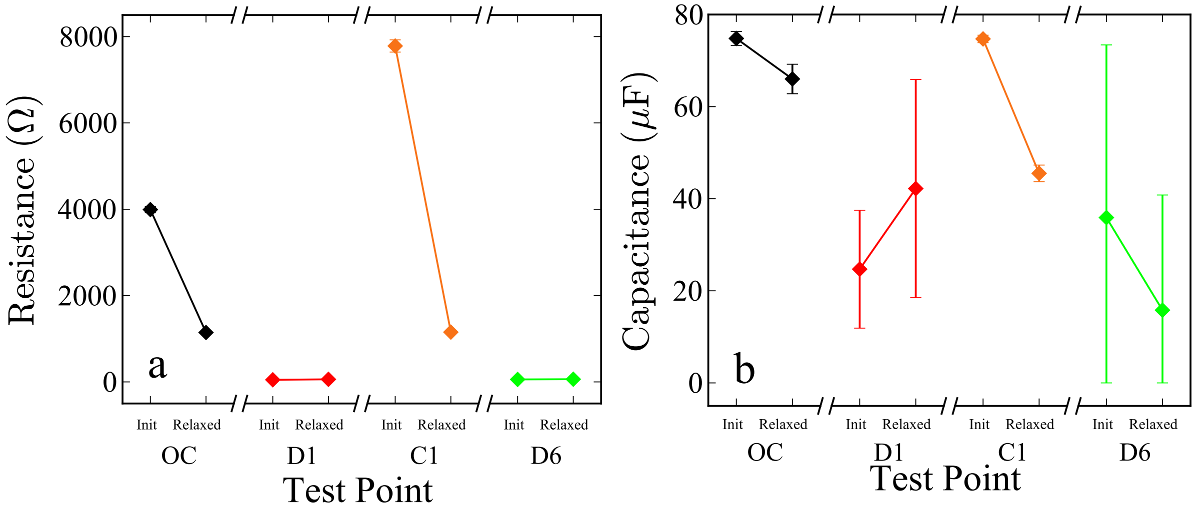

Figure S2. Time evolution of fitted impedance parameters for the equivalent circuit element corresponding to the a-Si thin-film. (a) Resistance values. (b) Pseudo-capacitance values, calculated according to equation 3 in the main manuscript. "Init" refers to EIS data taken immediately after the associated galvanostatic step (or immediately after cell assembly, for test point OC), and "Relaxed" refers to EIS data taken after several hours at open circuit. The open symbol for the final C1 data point represents EIS data taken only 21 minutes after charging, and hence is labeled "Partially Relaxed."

about these smaller capacitance differences. Future studies will explore the evolution of the a-Si electrochemical properties with extended cycling as a function of SOC.

Analysis of Irreversible Electrochemical Degradation with Half-cell Cycling

As shown in Figure 5 in the main body of the manuscript, the impedance for a given SOC increases slightly with increasing cycling; the impedance is larger at C1 than at OC and larger at D6 than at D1. Because the Nyquist plots maintain roughly the same shape as a function of SOC, this suggests that the magnitude of the arcs in the Nyquist plot increase proportionally. Figure 6 in the main body shows how R_{int} increases as a function of cycle number, with proportional increases accompanying each delithiation step. Figure S3 plots the EIS fitting parameters Q_{dl} and Q_{Si} for the two CPE elements as a function of SOC, where the impedance of the CPE is:

$$Z = \frac{1}{Q(j\omega)^n} \tag{S2}$$

with j the imaginary number. Results show that both values increase upon lithiation, relative to the previous delithiated state. However, upon delithiation to C1, the values do not return to their original value, but are 20-30% lower than at OC. This relative degree of degradation is preserved during the next lithiation step, but does not increase – the fitted values at D6 are also roughly 30% lower than at D1, indicating that anode degradation occurs predominantly upon delithiation. The roughly equal degradation effect spans multiple processes (i.e., 20-30% reduction of Q_{Si}, Q_{dl}, and $1/R_{\mathrm{int}}$) suggesting a loss of active anode area or volume, such as electrochemical isolation of some portion of the a-Si. However, this must be considered conservatively since the large error bars on Q_{Si}, (once again due to overlapping frequencies for the a-Si and

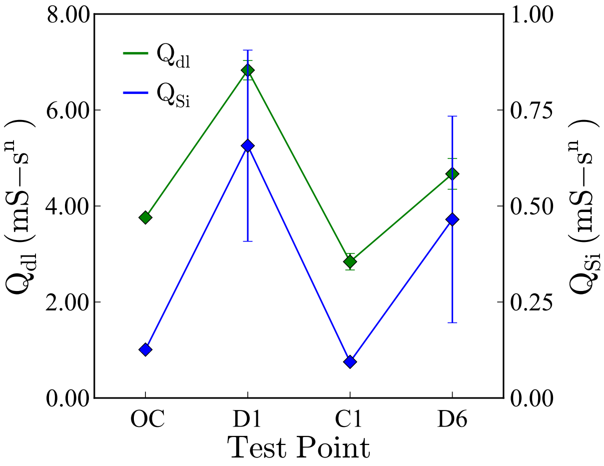

Figure S3. Variaiton of Q_{dl} and Q_{Si} vs. SOC. Results show that the values decrease by 20 to 30% after delithiation step C1, relative to the previous delithiated state (OC). The values increase by 44 to 87% upon lithiation, relative to the previous delithiated state.

double layer elements in the delithiated states) are larger than the difference between the values at D1 and D6.

Correction Factors for Substrate Warping:

Sample warping will tend to either focus or defocus the reflected neutron beam, and if defocussed sufficiently will cause a reduction of intensity entering the detector. However, for a fixed projection of the beam onto the sample, or footprint width, used for all but the smallest of incident angles, the effect of this warping is constant with θ. As mentioned in the main text, for 2θ ≤ 1°, specular scans were recorded with fixed slit widths, resulting in a projection of the beam onto the sample, or "footprint," that varies with θ. For the varying footprint at low angles, however, large enough sample warping will lead to systematic errors in the calculated reflectivity, with a higher warping effect at lower angles, due to the larger projected beam footprint. For this reason, scans with 2θ ≤ 1° (with the two upstream slits fixed at equal values during the scans) were repeated at 0.05 mm, 0.1 mm, and 0.2 mm. For these three scans the two downstream slits were fixed at 0.6 mm and 0.8 mm. For each scan, the reflected intensity was normalized by the incident intensity measured for the corresponding slit width. For a warp-free sample, the normalized intensities of each of these scans should not vary for all theta large enough that the projected beam footprint is totally contained within the sample width. For a warped sample, the effect of the warping (amount of focusing or defocusing) can vary as a function of the footprint, as the increasing footprint exposes surfaces with an increasing range of surface normal directions.

For the sample in this study, the warping varied with SOC, consistent with the compressive and tensile strains accompanying lithiation and delithiation, respectively. However, results demonstrated that the radius of curvature for the warping was not uniform across the sample, and the effect of the warping for each SOC varied as a function the footprint To correct for this non-uniform warping, the normalized constant slit scans were compared and were found to agree at higher angles (smaller footprint). For lower θ such that the footprint of the beam was larger than roughly 35-40mm the intensity was found to decrease relative to the other scans, indicating that the degree of warping was much greater beyond the central 35-40mm of the sample. The lower theta limit for consistent data was found for each constant slit scan and the data below this was discarded. For any theta range the data from the constant slit scan with largest available slit setting were used since they had higher neutron counts and lower relative errors. In some cases the normalized reflectivities were not equal but were only proportional to one another, implying a constant relative warping effect. For these regions, scan with smaller slit settings was scaled by the constant of proportionality before applying the preceding procedure. In this manner, θ regions unaffected by warping were identified for each slit setting, and warping was corrected in cases for which warping was constant. The uncertainty of these correction factors was propagated through the relatively small Q-range for which these corrections were applied. It should be noted, however, that some degree of systematic error from sample warp inevitably affects the data, particularly at these angles. While the beam focusing or defocusing due to warp is invariant at higher angles, any warping of the sample at these angles can influence the apparent instrument resolution and thus fitted NR parameters.

Interfacial Roughness/width Variations With SOC

The calculated values of roughness are shown in Table S2. The changes in interfacial roughness on either side of the AlO_x layer are roughly cyclic in nature, with the changes on either side of the layer offsetting one another; the electrolyte/AlO_x interface is rougher in the lithiated state and smoother in the de-lithiated state, while the AlO_x/a-Si interface is smoother in the lithiated state and rougher in the delithiated state. While it is possible that these changes are

Table S2. Best fits and 68% confidence intervals (in brackets) for interfacial roughness at each test point, obtained from NR fitting. *SiO_2 roughness values for test points C1-C6 were held fixed at the value simultaneously fit to test points OC and D1.

	Interface			
Test Point	SiO_2/Cu	Cu/a-Si	a-Si/AlO_x	AlO_x/Electrolyte
OC	0.13 [0.01, 0.29]	2.03 [1.88, 2.14]	0.56 [0.00, 0.92]	0.97 [0.77, 1.66]
D1	0.13 [0.01, 0.29]	1.45 [1.36, 1.55]	1.60 [1.28, 1.73]	0.16 [0.00, 0.56]
C1	0.13*	1.76 [1.66, 1.87]	0.56 [0.36, 1.34]	1.11 [0.91, 1.92]
D6	0.13*	1.56 [1.49, 1.62]	1.59 [1.23, 1.73]	0.17 [0.00, 0.56]
C6	0.13*	1.70 [1.62, 1.74]	0.44 [0.34, 0.97]	0.10 [0.00, 0.80]

either a fitting artifact or due to the volume expansion and contraction of the Si anode during discharge and charge, respectively, it is also possible that these cyclic changes are due to the internal stress and subsequent warping of the anode during lithiation and de-lithiation. Comparison of the repeated θ-scans below the critical angle showed evidence of significantly greater substrate warping for the discharged (lithiated) test points D1 and D6, relative to the de-lithiated test points OC, C1, and C6. This is presumably due to the internal compressive stresses that develop with lithium insertion, as documented by Sethuraman, et al[1]. Because warping changes the angular distribution of the incident and reflected beam, similar to instrumental broadening, it can alter the convolution of the oscillations in the reflectivity and effectively alter their amplitude. This effect could also be produced by larger interface roughness. Therefore, changes to the sample warping could easily be misconstrued as changes to the interfacial width between two layers of contrasting SLD. In this case, we are currently not able to identify whether the fitted roughness variation reflects physical changes due to warping or are fitting artifacts due to systematic bias. Subsequent investigations on samples less prone to warp will help elucidate more clearly the source and implications of these roughness changes for the AlO_x layer. We can, however, speculate at this point that the roughening of the interface is not due to roughening of the Si layer as a whole with AlO_x being conformal to it, because in that case we would see equal roughening at both Si/AlO_x and the AlO_x/Electrolyte interface, instead of the offsetting variations observed here.

Measurement of a-Si Density and Porosity:

In order to calculate the porosity of the as-deposited sample via equation 6, it is necessary to have an estimate of the SLD of the solid domains, which, in turn, requires an accurate estimate of the mass density ρ of the solid a-Si domains. An additional sample was thus fabricated, but with no AlO_x capping layer to allow more facile permeation of liquid into the pores, and NR was used to directly measure the porosity and SLD of the a-Si layers fabricated for this study. NR measurements were performed on the Horizontal Sample Neutron Reflectometer on beam line NG7 at the NIST Center for Neutron Research. This sample was measured first in air and then in a wet cell filled with D_2O (similar to the wet cell in Figure 1(b), but with no counter electrode). Given the low density of air, its effective SLD is zero, so the fitted SLD of the a-Si layer can be interpreted as:

$$SLD_{Si,air} = \phi SLD_{air} + (1-\phi)SLD_{a-Si-s} = (1-\phi)SLD_{a-Si-s} \tag{S3}$$

whereas in the second measurement the pores are filled with D_2O:

$$SLD_{Si,D2O} = \phi SLD_{D2O} + (1-\phi)SLD_{a-Si-s} \tag{S4}$$

Given the known value of SLD_{D2O} (6.36 × 10^{-4} nm^{-2}), equations S3 and S4 can be used to solve for $SLD_{a\text{-}Si}$. The fitted SLDs were $SLD_{Si,air}$ = 1.96 [1.94, 1.97]*10^{-4} nm^{-2} and $SLD_{Si,D2O}$ = 2.1 [2.10, 2.13]*10^{-4} nm^{-2}, resulting in an $SLD_{a\text{-}Si}$ value of 2.01 [2.00, 2.02] *10^{-4} nm^{-2}, and a as-deposited porosity in the AlO_x-capped sample of 10.0 [5.4, 28.0] %. This agrees well with the roughly 8% porosity estimated by comparing the quartz crystal microbalance measurements during film deposition and the NR-fitted thickness of the as-deposited sample.

References

(1) Sethuraman, V. A., Chon, M. J., Shimshak, M., Srinivasan, V. & Guduru, P. R. In situ measurements of stress evolution in silicon thin films during electrochemical lithiation and delithiation. *Journal of Power Sources* **195**, 5062-5066 (2010).

(2) Brodsky, M. H., Kaplan, D. & Ziegler, J. F. DENSITIES OF AMORPHOUS SI FILMS BY NUCLEAR BACKSCATTERING. *Applied Physics Letters* **21**, 305-& (1972).

(3) Renner, O. & Zemek, J. DENSITY OF AMORPHOUS SILICON FILMS. *Czechoslovak Journal of Physics* **B 23**, 1273-1276 (1973).

(4) Custer, J. S., Thompson, M. O., Jacobson, D. C., Poate, J. M., Roorda, S., Sinke, W. C. & Spaepen, F. DENSITY OF AMORPHOUS SI. *Applied Physics Letters* **64**, 437-439 (1994).